Smart Structures and Systems, *Vol. 27, No. 1 (2021) 101-114*
DOI: https://doi.org/10.12989/sss.2021.27.1.101

Damage detection for decks of concrete girder bridges using the frequency obtained from an actively excited vehicle

Jian Zhang [a], Chun-Xu Qu [b], Ting-Hua Yi* and Hong-Nan Li [c]

School of Civil Engineering, Dalian University of Technology, Dalian 116023, China

(*Received May 2, 2020, Revised November 8, 2020, Accepted November 12, 2020*)

Abstract. Concrete bridge decks may suffer local damage such as delamination, cracking, reinforcement corrosion and spalling during service. Visual inspection and nondestructive evaluation (NDE) technologies are extensively used for monitoring damage in bridge decks. This paper presents a damage detection method for decks of concrete girder bridges using the frequency obtained from an actively excited vehicle. First, the solution for the frequency of the deck with a concentrated mass is derived with Rayleigh's method, where the bridge deck is regarded as a slab supported on four sides, and the test vehicle is simplified as a concentrated mass. The validity of the proposed method that uses the frequency change to detect the local damage is verified. Then, the damage detection procedure for bridge decks is proposed, and the numerical analysis is performed on a typical concrete girder bridge to prove the validity of the method. Finally, the damage detection experiment for the plywood plate verifies the effectiveness of the proposed method. The results of this study provide an effective method for detecting damage in the decks of concrete girder bridges, which is time-saving and easier to implement.

Keywords: damage detection; bridge deck; actively excited vehicle; frequency change; Rayleigh's method

1. Introduction

The deterioration in concrete bridge decks is one of the concerns for the highway agency. Because of material degradation and high traffic loads, concrete bridge decks may suffer local damage, such as delamination, cracking, reinforcement corrosion and spalling (Yang *et al*. 2017, Fathalla *et al*. 2018, Raja *et al*. 2020). Visual inspection is a subjective method of evaluating concrete structures (Park *et al*. 2001, Estes and Frangopol 2003, Adhikari *et al*. 2014). The main drawback of visual inspections is that structural defects can only be detected when they can be clearly observed. Sometimes the damage to the inner layer of concrete is already so severe, with only tiny cracks on the surface (Graybeal *et al*. 2002). Meanwhile, it is difficult to perform an inspection on the bottom of a bridge deck on a stream or river (Rehman *et al*. 2016). Furthermore, the performance of NDE technologies has been validated on bridges in the SHRP 2 R06-A program, and different NDE technologies are tested in various situations, including impact echo (IE), ground penetrating radar (GPR), ultrasonic pulse echo (UPE) and so on (Gucunski *et al*. 2013). Most of these detection techniques are effective for the damage of the concrete near the surface. Nevertheless, these methods are difficult to detect internal damage away from the surface (Zhu and Popovic 2007). To evaluate the performance of the concrete structure and further maintenance, it is necessary to detect damage throughout the height of the section (Naito and Bolander 2019).

In addition to the above visual inspection and NDE technologies, vibration-based damage identification methods have been widely researched, and many damage indexes and algorithms were proposed (Yan *et al*. 2007, Kim *et al*. 2007, Fan and Qiao 2011, Tributsch and Adam 2018). In the dynamic test, the structure generates vibration under excitation, and its response is measured with transducers. Modal parameters such as natural frequency, mode shape and modal damping values are obtained (Faravelli *et al*. 2011, Shokrani *et al*. 2018). Once the structure deteriorates, the values of these modal parameters will change. Traditional vibration testing usually requires the installation of sensors in the field, which is inconvenient. Yang *et al*. (2004, 2014) separated the natural frequency and mode of the structure from the response of the moving vehicle. This method only needs to install an acceleration sensor on the vehicle to achieve the extraction of structural dynamic parameters. Oshima *et al*. (2014) extracted the mode shapes of the beam from the response of passing vehicles to further identify the damage of the beam. Xiang *et al*. (2010) proposed a damage detection method for moving vehicles equipped with a tapping device. Since the acceleration of the moving vehicle contains the local impedance of the bridge, the damage information can be extracted from the spectrum of the local dynamic response. Zhang *et al*. (2012) proposed to extract the mode shape square from the acceleration of the moving vehicle, and there is a sinusoidal excitation on the moving vehicle. Then, the damage location is determined by the mode shape square of the damaged and undamaged structures. Naito and

*Corresponding author, Professor,
E-mail: yth@dlut.edu.cn
[a] Ph.D. Candidate, E-mail: zj_001@mail.dlut.edu.cn
[b] Associate Professor, E-mail: quchunxu@dlut.edu.cn
[c] Professor, E-mail: hnli@dlut.edu.cn

ISSN: 1738-1584 (Print), 1738-1991 (Online)

Bolander (2019) used a vibrator to perform vibration tests on concrete members to detect the internal damage of concrete. There have been many researches on damage detection of bridges based on vehicle response, aiming at the detection of local cracking or stiffness reduction of one-dimensional simply supported or continuous beams. Small and medium-span bridges generally have a large width-to-length ratio and have different cross-sectional forms. It is not appropriate to simplify all of them to one-dimensional beams. It is necessary to carry out damage detection research according to the characteristics of specific types of bridges.

Among small and medium span bridges, a large number of concrete girder bridges were constructed, and the reinforced concrete deck was supported by several concrete girders (Jeon *et al*. 2012). In the design of bridge decks, the bridge deck is simplified as a plate on rigid girders, and rigid girders are regarded as the supports. This is because the flexural rigidity of the girder is many times higher than the flexural rigidity of the deck (Cao and Shing 1999, Han *et al*. 2003). According to the structural characteristics of a concrete girder bridges, the vibration modes of concrete girder bridges can be divided into two types: the global modes of vibration and local modes of vibration in the deck slab (Broquet *et al*. 2004).

Inspired by the vibration modes of girder bridges and previous studies, a damage detection method for a girder bridge decks are presented in this study. Local vibration of the bridge deck is excited by a shaker mounted on a vehicle, and the acceleration collected from the vehicle is processed to detect the local damage. The paper is organized as follows: First, for the simplified model of the deck with the test vehicle, the frequency change when a concentrated mass moves on the deck is studied based on Rayleigh's method. Then, the damage detection procedure for the deck of the concrete girder bridge is proposed. The numerical analysis is performed on a typical concrete girder bridge, and various damage conditions, such as delamination, section loss and cracking, are established in the model. Finally, the experiment is carried out in the laboratory to further verify the proposed method.

2. Damage detection of the deck using the frequency change

Because the local vibration of the bridge deck is of interest, the deck is supported by crossbeams, and two adjacent girders is cut out (Cao and Shing 1999, Han *et al*. 2003). The boundary conditions at the four sides of the deck take the place of the constraints between the deck and component, including the girders and crossbeam. The body and wheels of the test vehicle are all made of steel. The stiffness of the test vehicle is sufficiently large, and the test vehicle can be considered a rigid body. Therefore, the vehicle on the deck is simplified as a concentrated mass. The simplified model of the bridge deck with the test vehicle is shown in Fig. 1. First, the frequency of the deck with a concentrated mass is presented with Rayleigh's method. Then, the frequency change when a concentrated mass moves on the bridge deck is studied.

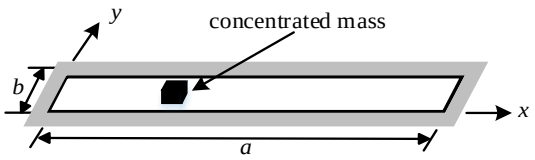

Fig. 1 Simplified model of the deck with the test vehicle

2.1 Frequency of the deck with a concentrated mass

According to Rayleigh's estimation method (Clough and Penzien 1975), an approximate solution for the frequency of the simplified model, as shown in Fig. 1, is proposed. The generalized mass m^* and generalized stiffness k^* are given by

$$m^* = \int_0^a \int_0^b m(x,y)\psi(x,y)^2 dxdy + M{\psi_M}^2 \tag{1}$$

$$k^* = D\int_0^a \int_0^b \left\{ \left[\frac{\partial^2 \psi(x,y)}{\partial x^2} + \frac{\partial^2 \psi(x,y)}{\partial y^2} \right]^2 - 2(1-\upsilon) \left[\frac{\partial^2 \psi(x,y)}{\partial x^2}\frac{\partial^2 \psi(x,y)}{\partial y^2} - \left(\frac{\partial^2 \psi(x,y)}{\partial y^2} \right)^2 \right] \right\} dxdy \tag{2}$$

Where $a =$ the length of the deck; $b =$ the width of the deck; $m(x,y) =$ the mass distribution per unit area; $\psi(x,y) =$ the shape function; $D = Eh^3/12(1-\upsilon^2) =$ the flexural rigidity of the deck; $\upsilon =$ the Poisson's ratio; $h =$ the thickness of the deck; $M =$ the concentrated mass; and $\psi_M =$ the value of the shape at the location of concentrated mass.

The generalized mass m^* and generalized stiffness k^* obtained from Eqs. (1) and (2) are substituted into Eq. (3) to obtain the frequency f of the deck with a concentrated mass.

$$f = \frac{1}{2\pi}\sqrt{\frac{k^*}{m^*}} \tag{3}$$

Obviously, as long as a proper shape function $\psi(x,y)$ is assumed, the frequency of the deck with a concentrated mass can be obtained. According to the selection principle of the shape function (Clough and Penzien 1975), the deflection shape $\omega(x,y)$ of the deck under the gravity load of the concentrated mass can be regarded as the approximate shape function $\psi(x,y)$.

First, it is assumed that the constraints at the four sides of the deck are simply supported, and the deflection shape $\omega(x,y)$ of the deck under the action of the concentrated load F is as defined in Eq. (4) (Timoshenko and Woinowsky-Krieger 1959). Point (ξ,η) is the location where the concentrated load F is applied. F is the gravity value of the concentrated mass. Then, the shape function

$\psi(x,y)$ is substituted with the deflection shape $\omega(x,y)$ in Eqs. (1) and (2). Finally, the frequency f of the deck with a concentrated mass can be obtained through Eq. (3).

$$\omega(x,y) = \frac{4F}{\pi^2 abD}\sum_{m=1}^{\infty}\sum_{n=1}^{\infty}\frac{\sin\frac{m\pi\xi}{a}\sin\frac{n\pi\eta}{b}}{\left(\frac{m^2}{a^2}+\frac{n^2}{b^2}\right)^2}\sin\frac{m\pi x}{a}\sin\frac{n\pi y}{b} \quad (4)$$

2.2 Frequency change of the deck with a moving mass

The change in the position of the concentrated mass on the deck is used to indicate the movement of the vehicle on the deck. Fig. 2 shows the shape function corresponding to the mass moving to different positions on the bridge deck. The shape function $\psi(x,y)$ is divided into three regions: R1, R2 and R3, as shown in Fig. 2, so Eq. (1) of the generalized mass m^* and Eq. (2) of the generalized stiffness k^* can be transformed into Eqs. (5) and (6). Because the value of the shape function of R1 and R3 is zero, the integration results of R1 and R3 are zero in Eqs. (5) and (6). Although the position of the integral region of R2 has changed, as shown in Fig. 2, the value of the shape function does not change, and the integration result of R2 is the same. Therefore, the values of m^* in Eq. (5) and k^* in Eq. (6) do not change when the concentrated mass is at different positions. From the above analysis, it can be concluded that the frequency of the deck with a concentrated mass remains unchanged as the concentrated mass moves across the undamaged deck.

$$m^* = \iint_{R_1} f_1(x,y)dA + \iint_{R_2} f_1(x,y)dA + \iint_{R_3} f_1(x,y)dA + M{\psi_M}^2 \quad (5)$$

$$k^* = D\left(\iint_{R_1} f_2(x,y)dA + \iint_{R_2} f_2(x,y)dA + \iint_{R_3} f_2(x,y)dA\right) \quad (6)$$

where

$$f_1(x,y) = m(x,y)\psi(x,y)^2 \quad (7)$$

$$f_2(x,y) = \left[\frac{\partial^2\psi(x,y)}{\partial x^2}+\frac{\partial^2\psi(x,y)}{\partial y^2}\right]^2 - 2(1-\upsilon)\left[\frac{\partial^2\psi(x,y)}{\partial x^2}\frac{\partial^2\psi(x,y)}{\partial y^2} - \left(\frac{\partial^2\psi(x,y)}{\partial y^2}\right)^2\right] \quad (8)$$

To verify the conclusion that the frequency of the deck with a concentrated mass remains unchanged as the concentrated mass moves across the undamaged deck, three cases are studied using Rayleigh's method and the finite element method (FEM). The following properties are adopted for the deck: length $a = 20$ m, width $b = 2$ m, thickness $h = 0.1$ m, and Young's modulus $E = 27.5$ GPa. The concentrated mass is located at different positions from the left end of the deck. The constraints at the four sides of the deck are simply supported. The results of the cases are shown in Table 1. The shape function assumed in Rayleigh's method and the vibration mode shape calculated by the FEM for the three cases are shown in Fig. 3. To evaluate the influence of different boundary conditions, the boundary condition of the deck for the fixed support is also considered. The frequency when the concentrated mass is located at different positions on the deck is shown in Table 1. It is difficult to obtain the expression of vibration shape

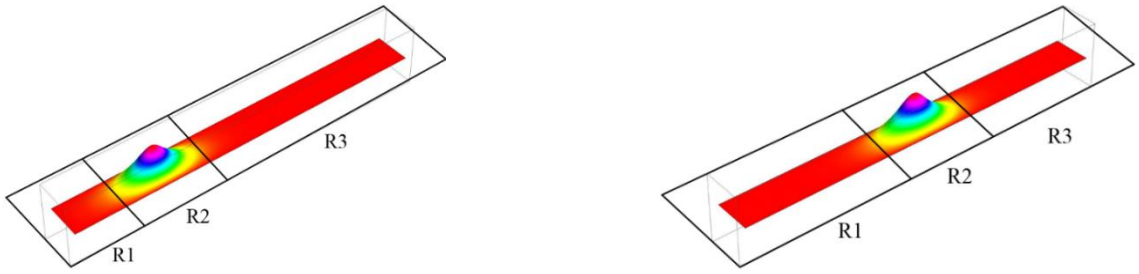

(a) The concentrated mass is in a certain location (b) The concentrated mass is in a different location

Fig. 2 Area division of the shape function

Table 1 Frequency of the deck with a concentrated mass obtained by Rayleigh's method and the finite element method

Case	Concentrated mass M (kg)	Concentrated mass location (m)	Simple support			Fixed support
			Rayleigh's method f_R (Hz)	FEM f_{FE} (Hz)	$\frac{f_R - f_{FE}}{f_{FE}}$ (%)	FEM f_{FE} (Hz)
1	500	5.0	33.393	32.157	3.844	56.915
2	500	7.5	33.393	32.147	3.876	56.915
3	500	10	33.393	32.147	3.876	56.915

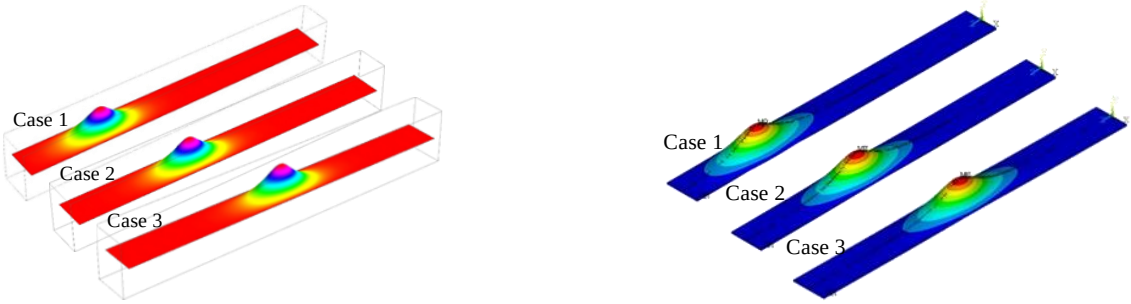

(a) Shape function (b) Vibration mode shape

Fig. 3 Shape function assumed in Rayleigh's method and vibration mode shape calculated by the FEM

similar to Eq. (4) under fixed-support boundary conditions, so only the results of the finite element method are given.

The shape function $\psi(x,y)$ assumed in Rayleigh's method determines the accuracy of the vibration frequency, and the mode function $\psi(x,y)$ represents the vibration mode shape (Clough and Penzien 1975). The frequency calculated by the FEM is used as a reference. It can be seen from Table 1 that the error in the frequency obtained by Rayleigh's method is small. The shape function assumed in Rayleigh's method and the vibration mode shape calculated by the FEM are close, as shown in Fig. 3. The results demonstrate that the shape function $\psi(x,y)$ assumed in Rayleigh's method is acceptable. The results in Table 1 also show that there is no change in the frequency obtained by the two methods with the change in the position of the concentrated mass. The results are consistent with the conclusion we have obtained above.

In fact, since the flexural rigidity of the girder is many times higher than the flexural rigidity of the bridge deck (Cao and Shing 1999, Han *et al*. 2003), the constraint between the deck and the girder is closer to the fixed support than the simple support. Under fixed boundary conditions, it can be concluded from Table 1 that the frequency of the deck with a concentrated mass remains unchanged as the position of the concentrated mass changes. This is consistent with the conclusion drawn when the boundary condition of the deck is simply supported. In consequence, the suitable condition for the above conclusion is not limited to the simply supported constraint and can be extended to other constraint conditions. If the boundary conditions of the deck change, only the shape function $\psi(x,y)$ changes when Rayleigh's method is used to obtain the frequency.

If the deck near the moving concentrated mass has local damage, the flexural rigidity of R2 is reduced. The local damage also leads to the modification of the shape function. According to Eqs. (5) and (6), the generalized mass m_d^* and generalized stiffness k_d^* of the damaged deck can be expressed as

$$m_d^* = \iint_{R_1} f_{1d}(x,y)dA + \iint_{R_2} f_{1_d}(x,y)dA + \iint_{R_3} f_{1d}(x,y)dA + M{\psi_M}^2 \tag{9}$$

$$k_d^* = D_d\left(\iint_{R_1} f_{2_d}(x,y)dA + \iint_{R_2} f_{2_d}(x,y)dA + \iint_{R_3} f_{2_d}(x,y)dA\right) \tag{10}$$

where D_d and $\psi_d(x,y)$ denote the flexural rigidity and shape function of the damaged deck.

$$f_{1d}(x,y) = m(x,y)\psi_d(x,y)^2 \tag{11}$$

$$f_{2_d}(x,y) = \left[\frac{\partial^2\psi_d(x,y)}{\partial x^2} + \frac{\partial^2\psi_d(x,y)}{\partial y^2}\right]^2 - 2(1-\upsilon)\left[\frac{\partial^2\psi_d(x,y)}{\partial x^2}\frac{\partial^2\psi_d(x,y)}{\partial y^2} - \left(\frac{\partial^2\psi_d(x,y)}{\partial y^2}\right)^2\right] \tag{12}$$

Similarly, the integration results of R1 and R2 are still zero, and only the integration result of R2 has a value. The frequency of the damaged deck with a concentrated mass can be expressed as

$$f_d = \frac{1}{2\pi}\sqrt{\frac{k_d^*}{m_d^*}} \tag{13}$$

Compared to the undamaged deck, Eq. (13) shows that the frequency change is obvious for the damaged deck. From the above analysis, it is concluded that if the concentrated mass approaches the local damage area on the deck, then the frequency of the deck with a concentrated mass changes. Previously, it was concluded that the frequency of the deck with a concentrated mass remains unchanged as the concentrated mass moves across the undamaged deck. Therefore, the frequency change can be used to detect the local damage of the bridge deck.

2.3 Procedure of damage detection

For the concrete girder bridge, the vibration of the deck is a high-order mode vibration of the bridge. To excite the vibration of the deck, it is necessary to apply a controllable excitation on the test vehicle. The test vehicle is equipped with a shaker as the active excitation to meet the excitation requirements. The frequency of the deck with the test vehicle can be obtained from the acceleration of the actively excited vehicle. As mentioned earlier, the body and wheels

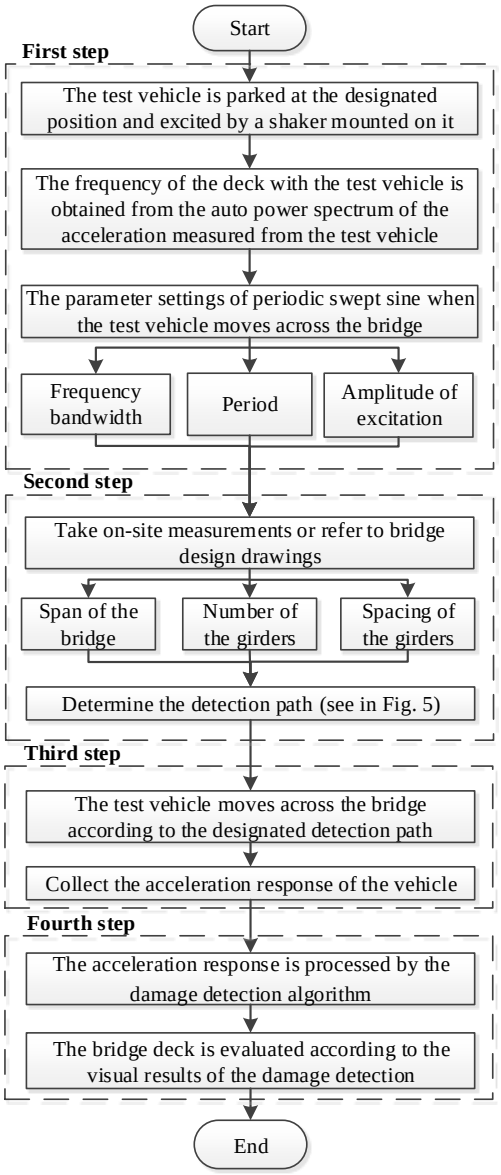

Fig. 4 Flow chart of the damage detection procedure

of the test vehicle are made of steel and there is no spring suspension system. Therefore, the natural frequency of the vehicle is very large and the vehicle can be regarded as a rigid body. The acceleration measured on the vehicle is the same as the acceleration measured at the point of contact between the vehicle and the deck. Consequently, the frequency obtained from the vehicle is the same as the frequency of the bridge deck near the vehicle. At this time, the test vehicle with the sensor can be regarded as an accelerometer with a large mass. The steps of the damage detection procedure are as follows (see Fig. 4).

Step (1): Set the excitation parameters before detection. Before carrying out the damage detection of the deck, it is necessary to determine the excitation scheme in advance. To continuously excite the vibration mode, as shown in Fig. 3, as the vehicle moves across the bridge, periodic swept sine excitation is applied to the moving test vehicle. Swept sine testing is a widely accepted test technique in the industry. During the test, the sine wave will sweep from the low frequency to the high frequency with time (Avitabile 2018). Excitation parameters, including the frequency bandwidth, period and amplitude of excitation, need to be set before the detection.

To excite the vibration mode of interest, the bandwidth of the excitation must cover the vibration frequency of the deck with the test vehicle, which is called f_{vd}. The f_{vd} of the on-site bridge is unknown before detection, so swept sine excitation is required to determine the value of f_{vd} in advance. The test vehicle is parked in the middle of the deck between two adjacent girders (see Fig. 5), and then the vehicle is excited by the shaker mounted on it. At the same time, the acceleration response of the vehicle is collected. The frequency f_{vd} is obtained from the auto power spectrum of the acceleration measured from the test vehicle. Using f_{vd} as the centre frequency of the bandwidth ensures that the vibration mode of interest can be excited. The upper and lower limits of the bandwidth are determined by the change in f_{vd} caused by the damage of the deck. According to the numerical analysis of different damage levels and types of bridge decks, the frequency reduction due to local damage does not exceed 15% of f_{vd}. Therefore, it is recommended that the upper limit of the bandwidth be taken as the center frequency plus 15%-20%, and the lower limit of the bandwidth be taken as the center frequency minus 15%-20%. The distance traveled by the vehicle on the deck during a period of the excitation is a detection segment, so the period of the excitation and the speed of the vehicle determine the length of the detection segment. The amplitude of the excitation depends on the range of the excitation force provided by the type of shaker.

Step (2): Determine the detection path. According to the design drawings or on-site measurements, the span of the bridge, number of girders and spacing of the two adjacent girders are acquired. Then, the detection path of the test vehicle can be determined. The vehicle travels along the

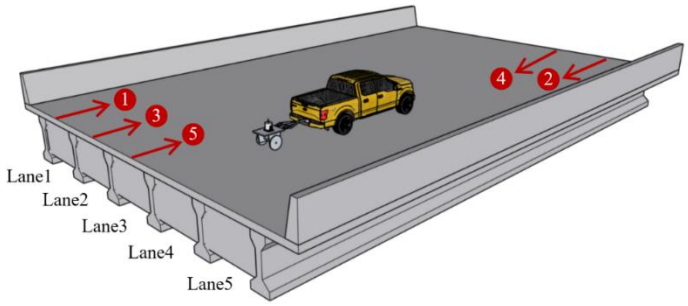

Fig. 5 Determined detection path

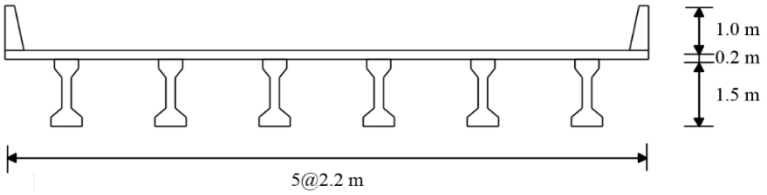

Fig. 6 Cross section of the bridge

centerline of two adjacent girders during the test, which is the direction shown by the arrow in Fig. 5. The detection of all lanes is performed in the order marked in Fig. 5.

Step (3): Test vehicle moves across the bridge. The test vehicle moves from one end to the other of the bridge according to the detection path set by the second step. At the same time, the excitation is applied to the vehicle by the shaker according to the parameters set by the first step. The acceleration response of the vehicle is synchronously collected by the accelerometer mounted on the test vehicle.

Step (4): Obtain visual results of the damage detection. The acceleration response of the vehicle contains damage information of the bridge deck. The acceleration is processed by the damage detection algorithm, and visual results of the damage detection are shown. The algorithm consists of the following steps.

In the first step, the measured acceleration signal is divided into equal segments, and each data segment represents a detection segment. The length of each segment is the same as the period of the excitation during the test to ensure that the excitation force is the same in each segment. For example, the signal in the time domain is divided into n segments. In the second step, the auto power spectrum is computed for the segmented acceleration response. N number of the auto power spectrum will be obtained by n segments. In the third step, the amplitude of each auto power spectrum is sampled at equal intervals to form a vector, and a total of n vectors are obtained. In the fourth step, for any two vectors $\boldsymbol{V_i}$ and $\boldsymbol{V_j}$, the value of Q is calculated according to Eq. (14). The value of Q is used to indicate the degree of similarity between the two vectors. A square matrix of order n is obtained by n vectors. The values in the square matrix represent the differences in the vibration frequency of the test vehicle between any two detection segments. If the stiffness of the bridge deck is not abnormal, the value of Q is 1. Conversely, if the stiffness of the bridge deck is abnormal, the value of Q will be less than 1. In the fifth step, the visualization of the results is performed. The square matrix obtained in the previous step is integrated with positioning data to generate the contour plot of the scanned deck.

$$Q(i,j) = \frac{\left(\boldsymbol{V_i} \cdot \boldsymbol{V_j}\right)^2}{\left(\|\boldsymbol{V_i}\| \times \|\boldsymbol{V_j}\|\right)^2} \quad i,j = 1,2,\cdots,n \tag{14}$$

3. Numerical analysis of the bridge detection procedure

This section uses numerical simulations to verify the effectiveness of the proposed method. The deck of a typical concrete girder bridge is detected by the damage detection procedure. The local damage of the deck is modelled as the delamination, section loss and cracking.

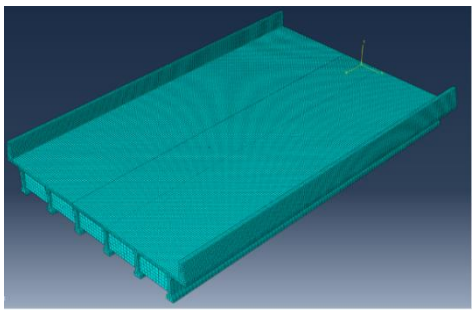

Fig. 7 Finite element model of the bridge

3.1 Numerical modeling

The bridge has a roadway width of 13.30 m and a bridge deck thickness of 0.20 m, as shown in Fig. 6. The span of the bridge is 20 m. The number of crossbeams is three, which are located at the end and middle of the bridge. The bridge is modeled with ABAQUS software using solid elements. Fig. 7 shows the finite element model of the bridge. Its material properties are as follows: elastic modulus $E = 27.5$ GPa and mass density $\rho = 2400$ kg/m^3; the damping ratio is assumed to be 0.02. The test vehicle is simplified as the spring mass damping system, as shown in Fig. 8. The mass of the car body is $m_v = 400$ kg, the mass of the wheel is $m_v = 100$ kg, the spring stiffness is k_v=1e6 kN/m and the damping ratio is $c = 0.02$. The frequency f_{vd} of the deck with the test vehicle is obtained by swept sine excitation in the first step of damage detection. The excitation parameters are as follows: the total time of excitation is 5 s, the frequency bandwidth is 50 Hz-150 Hz, and the amplitude is 0.1 kN. The periodic swept sine excitation is applied to the vehicle to continuously excite the bridge deck while the vehicle travels across the bridge. The excitation parameters are as

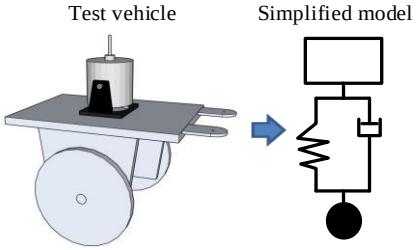

Fig. 8 Model of the test vehicle

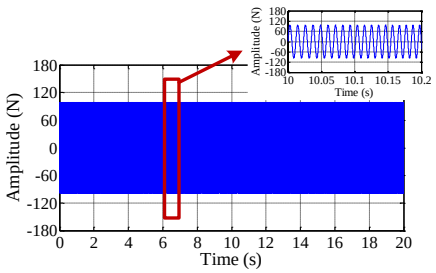

Fig. 9 Excitation signal applied on the vehicle during damage detection

follows: the period of excitation is 0.4 s, the frequency bandwidth is 80 Hz - 120 Hz, and the amplitude is 0.1 kN. The speed of the test vehicle is 1 m/s. The time that it takes for the vehicle to drive across the bridge is 20 s. The excitation signal applied on the vehicle during the detection is shown in Fig. 9.

3.2 Damage scenarios of the deck

In the current research on bridge damage identification, structural damage is generally simulated as the stiffness reduction of the element, and the degree of damage is characterized according to the percentage and range of stiffness reduction. It is a challenge to establish the relationship between the actual damage conditions and the stiffness reduction. In this study, the bridge is modeled by solid elements, which can be characterized in more detail. Therefore, various damage conditions, such as delamination, section loss and cracking, are established in the model rather than the stiffness reduction of the element. The delamination is modeled as the disconnection of elements at a certain height in the range of the damage. The section loss is modeled as the elimination of elements with a certain thickness at the bottom of the deck. The cracking is modeled as the disconnection of the element at the crack of the deck.

The damage scenarios of delamination and section loss are set in each lane, as shown in Fig. 10. The location and size of the local damage are shown in Table 2. The delamination is located in the middle of the section, and the distance from delamination to the top surface of the bridge deck is 0.1 m. The section loss is the destruction of the concrete on the bottom surface of the deck, which is caused by the spalling of the concrete cover for the reinforcement.

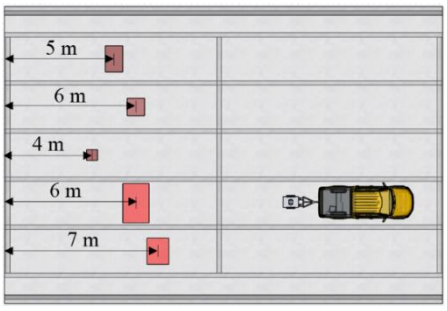

Fig. 10 Damage scenarios for delamination and section loss are set in each lane

The thickness of the concrete cover is 0.04 m.

Damage scenarios of cracks in the longitudinal and transverse directions are set in each lane, as shown in Fig. 11. The location and size of the crack in each scenario are shown in Table 3. The cracks are on the bottom surface of the bridge deck. The crack depth is 0.1 m, which is half the thickness of the deck. The above damage conditions are common in bridge decks, and local damage located far from the top surface. For most of NDE technologies, it is difficult to detect the damage from the top surface of the bridge deck.

3.3 Results analysis of damage detection

To obtain the frequency f_{vd} of the deck with the test vehicle in the first step of damage detection, swept sine excitation is applied to the test vehicle. The acceleration response of the vehicle is measured, as shown in Fig. 12. The auto power spectrum of the response is given in Fig. 13. The frequency corresponding to the highest peak in the spectrum is 99.71 Hz, which is f_{vd}. In addition, the modal analysis of the bridge is carried out using ABAQUS

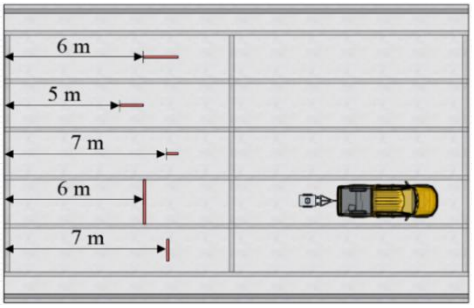

Fig. 11 Damage scenarios of the cracks in the longitudinal and transverse directions in each lane

Table 2 Damage scenarios of delamination and section loss

Lane	Damage scenario	Damage location (m)	Damage size (m)
1	Delamination	5.0	0.8 × 1.2
2	Delamination	6.0	0.8 × 0.8
3	Delamination	4.0	0.5 × 0.5
4	Section loss	6.0	1.2 × 1.8
5	Section loss	7.0	1.2 × 1.2

Table 3 Damage scenarios of the cracks in the longitudinal and transverse directions

Lane	Damage scenario	Damage location (m)	Damage size (m)
1	Longitudinal crack	6.0	1.5
2	Longitudinal crack	5.0	1.0
3	Longitudinal crack	7.0	0.5
4	Transverse crack	6.0	2.0
5	Transverse crack	7.0	1.0

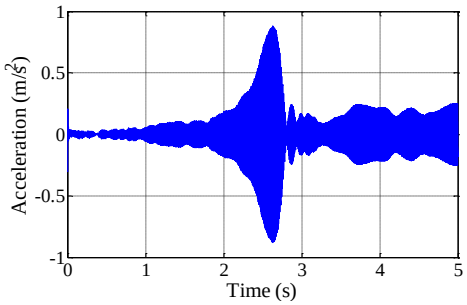

Fig. 12 Acceleration response measured from the vehicle in the first step of damage detection

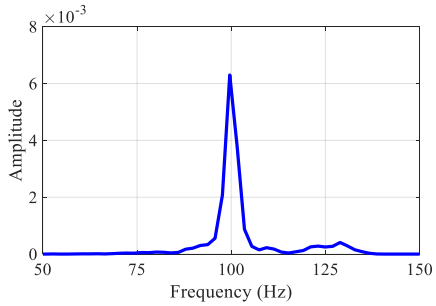

Fig. 13 Auto power spectrum of the response measured from the vehicle in the first step of damage detection

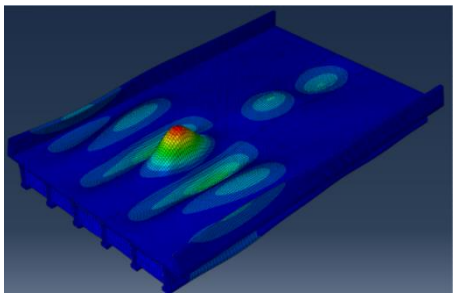

Fig. 14 Mode shape of the vibration corresponding to the frequency of the deck with the test vehicle

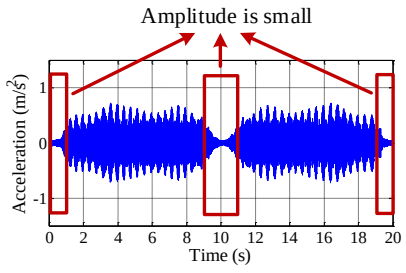

Fig. 15 Typical acceleration response measured from the vehicle as the vehicle travels across the bridge

software, and the mode of vibration shown in Fig. 14 can be found. The frequency of the modal analysis in ABAQUS is 99.82 Hz, which is consistent with the frequency value obtained in the auto power spectrum. The mode shape in Fig. 14 also corresponds to the shape function of the simplified model.

As the test vehicle travels across the bridge, the typical acceleration response measured from the wheel or body of the test vehicle is shown in Fig. 15. Since the stiffness of the vehicle is sufficiently large and the vehicle can be regarded as a rigid body, the acceleration measured from the wheel and body of the vehicle are the same. It is observed from the waveform of the acceleration that the periodic swept sine excitation excites a certain order of vibration mode. Due to the existence of the crossbeams at the end of the bridge, the amplitude of the acceleration of the vehicle is small when the test vehicle moves at the two ends of the bridge (see Fig. 15). Similarly, there is a crossbeam in the middle of the bridge. The amplitude of the acceleration is also small when the vehicle is approaching the middle of the bridge (see Fig. 15). This is because the crossbeams cause a sudden change in the local stiffness of the deck. When the vehicle is approaching the crossbeams, the vibration mode shown in Fig. 14 cannot be excited.

The acceleration response of the vehicle collected in each lane is processed by the damage detection algorithm. Visual results for the damage scenarios of delamination and section loss are shown in Fig. 16. Due to the existence of the crossbeams, the anomaly occurs at the edge and middle of each contour plot. In addition, the location of the anomaly in the contour plot matches well with the location of the local damage in each lane (see Fig. 10). From the damage scenarios of Lane 1 to Lane 3, the delaminated area of the deck is gradually reduced, and the extent and range of the anomaly in the contour plot decreases. When the dimensions of the delamination are 0.5 m by 0.5 m in Lane 3, the anomaly in the contour plot is very small. If the delaminated area continues to decrease, damage cannot be detected. The anomaly in the contour plot occurs because the vibration frequency obtained from the vehicle changes as the vehicle approaches the damage area. The auto power spectrum of the response measured from the vehicle during one excitation period when the vehicle travels through damaged and undamaged areas in different lanes is shown in Fig. 17. The frequency corresponding to the highest peak in the spectrum is f_{vd}. It is shown that the frequency f_{vd} decreases as the degree of damage gradually increases. For the damage scenarios of section loss in Lane 4 and Lane 5, the visual results also show anomalies at the location of the damage.

The visual results for the damage scenarios of cracks in the longitudinal and transverse directions are shown in Fig. 18. As the crack length decreases, the extent and range of the anomaly in the contour plot is also reduced. The crack length of the deck is 1 m in Lane 2 and Lane 5. The crack in the longitudinal direction can be detected, but the crack in the transverse direction cannot be detected. It can be concluded that the stiffness reduction of the deck by the crack in the longitudinal direction is greater than that of the crack in the transverse direction for the same crack length. To evaluate the performance of the concrete structure and further maintenance.

To evaluate the performance of concrete decks and further maintenance, it is necessary to detect damage throughout the height of the section. Current NDE

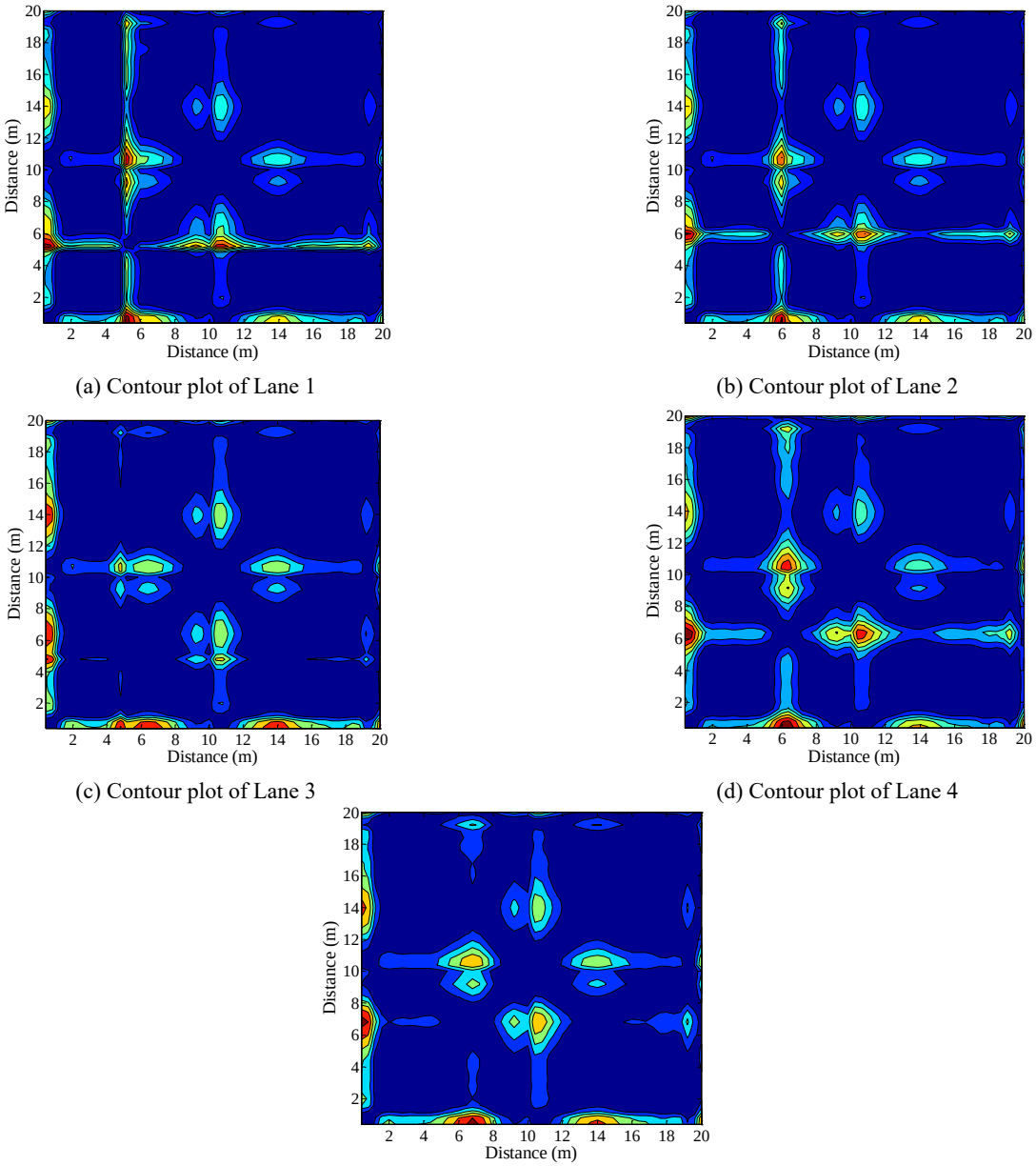

(a) Contour plot of Lane 1

(b) Contour plot of Lane 2

(c) Contour plot of Lane 3

(d) Contour plot of Lane 4

(e) Contour plot of Lane 5

Fig. 16 Visual results for delamination and section loss

technologies have good performances for detecting the damage of the concrete bridge deck near the surface, but the method proposed in this study can also detect local damage away from the surface. It is worth noting that NDE technologies are not limited to the type of bridges. However, this study focuses on detecting decks of concrete girder bridges, which is determined by the theoretical model.

It should be noted that the proposed method can determine the damage location based on the change of the vibration frequency of the vehicle, but hardly determine the specific type and extent of damage. It can be qualitatively concluded that the greater extent and range of the anomaly in the contour plot, the greater the extent of damage. The proposed method can quickly determine the location of the damage, then visual inspection and NDE technologies can

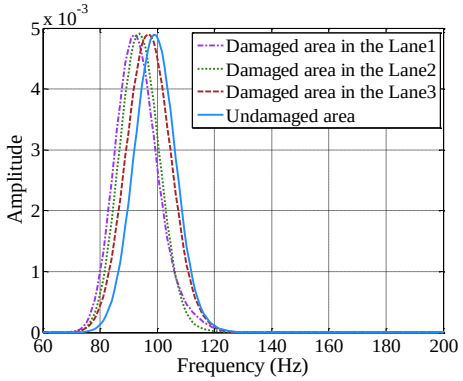

Fig. 17 Auto power spectrum of the response measured from the vehicle during one excitation period when the vehicle travels through damaged and undamaged areas in different lanes

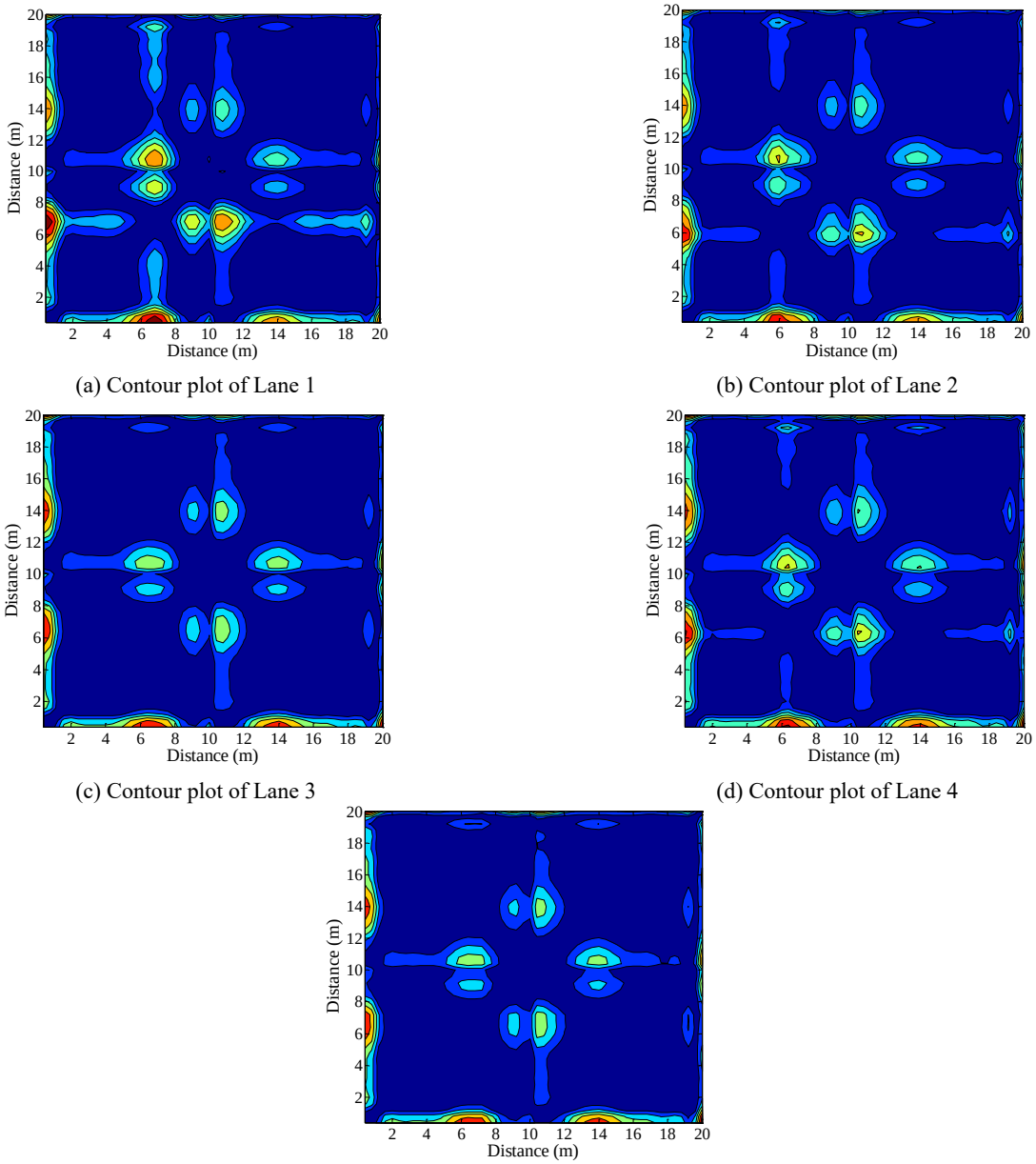

(a) Contour plot of Lane 1

(b) Contour plot of Lane 2

(c) Contour plot of Lane 3

(d) Contour plot of Lane 4

(e) Contour plot of Lane 5

Fig. 18 Visual results for the damage scenarios of cracks in the longitudinal and transverse directions

be used to determine the type and extent of the damage. To evaluate the potential of the proposed method for damage detection, the lower limit of detection for various types of damage is given by numerical analysis. For instance, the delamination with the size greater than 0.5 m × 0.5 m and the section loss (spalling of the concrete cover for the reinforcement) with the size greater than 1.2 m × 1.2 m can be detected.

3.4 Effect of the vehicle speed on damage detection

The speed of the test vehicle is an important factor that affects the detection efficiency. The effect of different vehicle speeds on the damage detection is studied in this section. The vehicle speed is set to 0.5 m/s, 1 m/s, 2 m/s, 4 m/s. As mentioned in the first step of the detection procedure, the period of the excitation and the speed of the vehicle determine the length of the detection segment. To ensure that the length of the detection segment is the same at different vehicle speeds. The period of the excitation corresponding to different speeds is set to 0.8 s, 0.4 s, 0.2 s, 0.1 s. The damage is set as the delamination with the size 0.8 m × 0.8 m, which is the same as the damage scenario of lane 2 in Table 2. The results of the damage detection at different vehicle speeds are shown in Fig. 19.

It can be seen from Fig. 19 that as the vehicle speed increases, the anomaly at the damage location is gradually not obvious in the contour plot. The result of detection becomes worse as the vehicle speed increases. The research on the sweep excitation points out that excessive sweep velocity cannot excite the quasi-steady state response of the

structure, which further leads to distortion of the frequency response function and auto power spectrum (Gloth and Sinapius 2004). In this study, the decrease of excitation period with the increase of vehicle speed, which leads to the increase of sweep velocity. The excessive sweep speed is not enough to excite the quasi-steady state response of the deck. Therefore, the result of damage detection becomes worse with the increase of sweep velocity. Through the above analysis, it is concluded that the speed of 1 m/s can ensure good detection results and maintain high detection efficiency at the same time.

4. Experimental verification

The experiment in the laboratory is carried out to further verify the proposed method. The detection of the plywood plate is performed according to the proposed procedure of damage detection.

4.1 Setup of the experiment

A plywood plate with sizes of $1.50\ \text{m} \times 0.35\ \text{m} \times 0.02\ \text{m}$ is shown in Fig. 20(a). Local damage ($0.35\ \text{m} \times 0.02\ m$), which is located in the middle of the plate, is

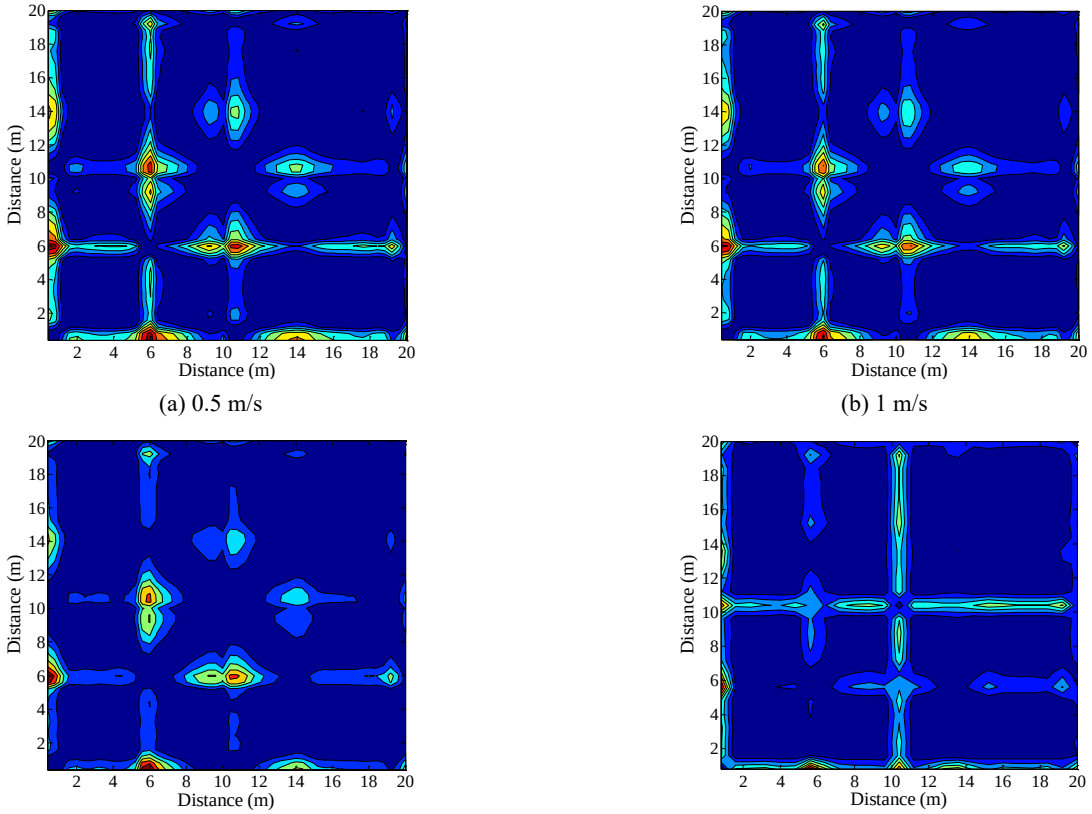

(a) 0.5 m/s (b) 1 m/s

(c) 2 m/s (d) 4 m/s

Fig. 19 Visual results of damage detection at different vehicle speeds

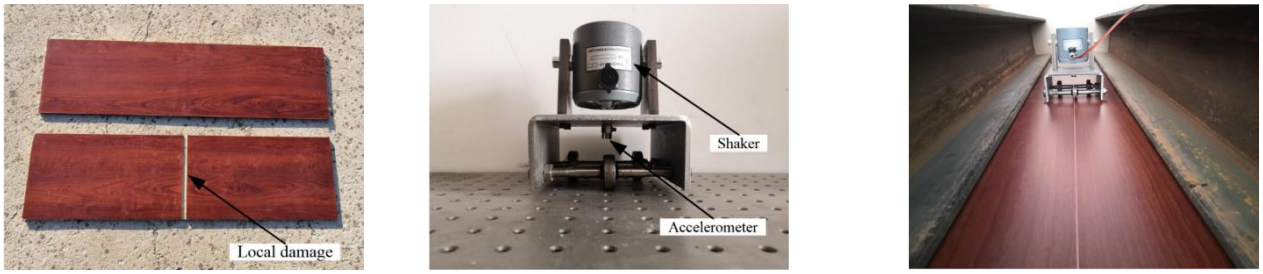

(a) Damaged and undamaged plywood plates

(b) Actively excited vehicle designed in the experiment

(c) The plywood plate is detected by an actively excited vehicle under the action of the traction motor

Fig. 20 Photograph of the experimental setup

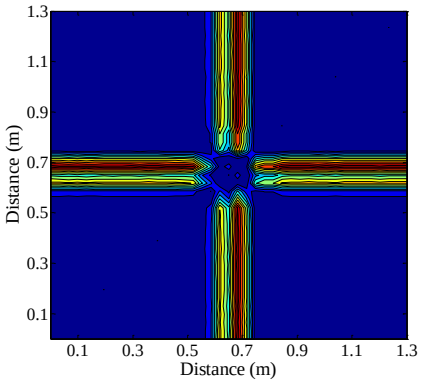

(a) Damaged plywood plates

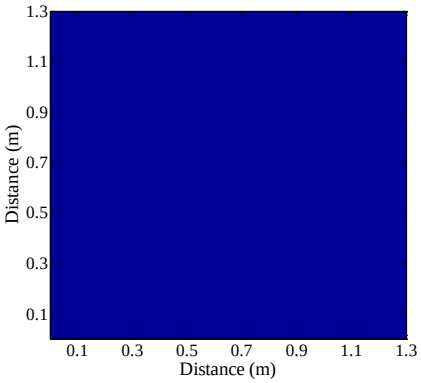

(a) Damaged plywood plates

Fig. 21 Visual results for damage detection

introduced artificially by reducing the thickness to 0.015 m (see Fig. 20(a)). The plywood plate is detected by an actively excited vehicle under the action of the traction motor, and the four sides of the plate are constrained, as shown in Fig. 20(c). A simple actively excited vehicle is used in the test, as shown in Fig. 20(b). The body and wheels of the vehicle are made of steel, which has the hard stiffness. A shaker is mounted on the body of the vehicle to provide periodic swept sine excitation. An accelerometer is fixed on the body of the vehicle to obtain the acceleration response. The frequency f_{vd} of the plate with the test vehicle is 87 Hz in the first step of damage detection. The actively excited vehicle passes along the centerline of the plate from the left end to the right end at a speed of 0.02 m/s during the experiment. The periodic swept sine excitation (frequency bandwidth from 67 Hz to 107 Hz with sweep period of 0.4 s) is applied to the vehicle by the shaker.

4.2 Experimental results

The visual results for the damage detection of the damaged plywood plate and the undamaged plywood plate are shown in Fig. 21. The length of the plywood plate is 1.5 m, and the length of the vehicle is 0.2 m, so the distance that the vehicle travels on the plate is 1.3 m. The visual result shows that the location of the anomaly in the contour plot matches well with the location of the local damage, as shown in Fig. 21(a). This indicates that the vibration frequency f_{vd} of the plate with the test vehicle changes when the vehicle approaches the damage area on the plywood plate. There is no anomaly in the visual result of the undamaged plywood plate (see Fig. 21(b)), so the frequency of the plywood plate with the vehicle remains unchanged as the vehicle moves across the plate. The experimental results are consistent with the conclusions drawn from the simplified model of the deck with the test vehicle.

5. Discussion of the proposed method in practical applications

The test vehicle is regarded as a rigid body in this study. Although the structure of the test vehicle is very simple, the detection vehicle has natural frequencies in multiple directions. To meet the requirement that the vehicle is a rigid body, it is necessary to reasonably design the vehicle so that the vertical natural frequency is much greater than the excitation frequency. Through simulation analysis, it is concluded that when the vertical frequency of the vehicle is more than 5 times the excitation frequency, the acceleration measured on the vehicle is the same as the acceleration measured at the contact point between the vehicle and the deck. At this time the vehicle itself does not vibrate but moves with the deck. In the design of the test vehicle, the structure should be simple, the wheels and the body should have great rigidity, and the connection between the wheels and the body should be very strong.

The damage of the deck below certain limits cannot be detected within real-world application. Such as the delamination with the size less than 0.5 m × 0.5 m, the section loss (spalling of the concrete cover for the reinforcement) with the size less than 1.2 m × 1.2 m, the longitudinal crack with the length less than 1 m and the transverse crack with the length less than 2 m. In addition, due to the crossbeam causes the sudden change in the local stiffness of the deck, the anomaly occurs at the contour plot. If the distance between the location of the damage and the transverse beam is less than half of the distance between two adjacent girders, the damage of the deck cannot be detected because of the interference of the crossbeam.

The temperature change can cause the bridge deck to shrink and expand, resulting in stress changes on bridge joints. In addition, the temperature change can also cause changes in the dynamic characteristics of the bridge by affecting the stiffness of the bridge. The specific mechanism mainly includes changes in the Young's modulus for the concrete and boundary conditions caused by the temperature change (Wahab and Roeck 1997, Liu and DeWolf 2007). The field testing measured temperatures of the bridge throughout a summer day (Mosavi *et al*. 2012). Results of the field testing showed that the temperature change is a slow process. The change in the temperature notably increased from night to noon. The maximum change occurred in the concrete deck (15.8°C), and the maximum change in one hour is about 2.5°C. In this study, the damage is detected by comparing the frequency change between the damaged and undamaged areas of the deck. According to the damage detection procedure, the damage

detection of the deck can be completed within a few minutes. The temperature change is very small during the detection process. Therefore, the temperature change has almost no effect on the effectiveness of the proposed method.

6. Conclusions

Concrete girder bridges are one of the forms of small and medium span bridges, and were built in large numbers worldwide. The damage of the deck is one of the main diseases of concrete girder bridges. The rapid detection of the bridge deck is of great significance to the safety of concrete girder bridges. This paper presents a novel damage detection method for decks of concrete girder bridges using the acceleration collected from an actively excited vehicle. First, for the simplified model of the deck with the test vehicle, the frequency change when a concentrated mass moves on the deck is studied based on Rayleigh's method. Then, the damage detection procedure for bridge decks is proposed, and the numerical analysis is performed on a typical concrete girder bridge. Finally, the experiment in the laboratory is carried out to further verify the proposed method. The following conclusions can be drawn:

- The bridge deck is regarded as a deck slab supported on four sides, and the test vehicle on the deck is simplified as a concentrated mass. The solution for the frequency of the deck with a concentrated mass is proposed based on Rayleigh's method. Then, the change in the position of the concentrated mass on the deck is used to indicate the movement of the vehicle on the deck. The frequency change when a concentrated mass moves on the bridge deck is studied. It can be concluded that the frequency of the deck with a concentrated mass remains unchanged as the concentrated mass moves across the undamaged deck. Notably, the frequency of the deck with a concentrated mass changes as the vehicle approaches the local damage area on the deck.
- According to the conclusions drawn from the simplified model of the deck with the test vehicle, the damage detection procedure for the deck is proposed. To excite the vibration of the deck with the test vehicle, the vehicle is equipped with a shaker as an active excitation source to meet the excitation requirements. The effectiveness of the proposed method is verified by the numerical simulation of a typical concrete girder bridge. The local damage of the deck is modeled as delamination, section loss and cracking. The above damage conditions are common and local damage located far from the top surface. For most of NDE technologies, it is difficult to detect the damage from the top surface of the bridge deck. The results show that the damage detection method is valid for different damage scenarios.
- The damage detection of the plywood plate is performed according to the method proposed in the laboratory. The local damage of artificial section loss on the plywood plate can be detected. The experimental results are consistent with the conclusions drawn from the simplified model of the deck with the test vehicle. Further research is ongoing to verify the applicability of the proposed method in field tests. In this study, the test vehicle is simplified as a concentrated mass; that is, the stiffness of the vehicle is large enough to be regarded as a rigid body. Therefore, in field testing, the design of a test vehicle that is consistent with that of the research needs to be considered in the future.

Acknowledgments

This research work was jointly supported by the National Natural Science Foundation of China (Grant Nos. 51625802, 51978128, 51778105), the LiaoNing Revitalization Talents Program (Grant No. XLYC1802035), and the Foundation for High Level Talent Innovation Support Program of Dalian (Grant No. 2017RD03).

References

Adhikari, R.S., Bagchi, A. and Moselhi, O. (2014), "Automated condition assessment of concrete bridges with digital imaging", *Smart Struct. Syst., Int. J.*, **6**(13), 901-925. https://doi.org/10.12989/sss.2014.13.6.901

Avitabile, P. (2018), *Modal testing: a practitioner's guide*, John Wiley & Sons Ltd., Hoboken, NJ, USA.

Broquet, C., Bailey, S.F., Fafard, M. and Bruehwiler, E. (2004), "Dynamic behavior of deck slabs of concrete road bridges", *J. Bridge Eng.*, **9**(2), 137-146. https://doi.org/10.1061/(ASCE)1084-0702(2004)9:2(137)

Cao, L.C. and Shing, P.B. (1999), "Simplified analysis method for slab-on-girder highway bridge decks", *J. Struct. Eng.*, **125**(1), 49-59. https://doi.org/10.1061/(ASCE)0733-9445(1999)125:1(49)

Clough, R.W. and Penzien, J. (1975), *Dynamics of Structures*, McGraw-Hill, New York, USA.

Estes, A.C. and Frangopol, D.M. (2003), "Updating bridge reliability based on bridge management systems visual inspection results", *J. Bridge Eng.*, **8**(6), 374-382. https://doi.org/10.1061/(ASCE)1084-0702(2003)8:6(374)

Fan, W. and Qiao, P.Z. (2011), "Vibration-based damage identification methods: a review and comparative study", *Struct. Health Monit.*, **10**(1), 83-111. https://doi.org/10.1177/1475921710365419

Faravelli, L., Ubertini, F. and Fuggini, C. (2011), "System identification of a super high-rise building via a stochastic subspace approach", *Smart Struct. Syst., Int. J.*, **7**(2), 133-152. https://doi.org/10.12989/sss.2011.7.2.133

Fathalla, E., Tanaka, Y. and Maekawa, K. (2018), "Remaining fatigue life assessment of in-service road bridge decks based upon artificial neural networks", *Eng. Struct.*, **171**, 602-616. https://doi.org/10.1016/j.engstruct.2018.05.122

Girgis, A.F.M. and Tadros, M.K. (2007), "Progress in structural engineering and materials: Concrete construction - Precast concrete bridge systems optimization", *Struct. Control Health Monit*, **14**, 522-536. https://doi.org/10.1002/stc

Gloth, G. and Sinapius, M. (2004), "Analysis of swept-sine runs during modal identification", *Mech. Syst. Signal Pr.*, **18**(6), 1421-1441. https://doi.org/ 10.1016/S0888-3270(03)00087-6

Graybeal, B.A., Phares, B.M., Rolander, D.D., Moore, M. and Washer, G. (2002), "Visual inspection of highway bridges", *J.*

Nondestruct. Eval., **21**(3), 67-83. https://doi.org/10.1023/A:1022508121821

Gucunski, N., Imani, A., Romero, F., Nazarian, S., Yuan, D. and Wiggenhauser, H. (2013), "Nondestructive testing to identify concrete bridge deck deterioration", Washington, D.C., Transportation Research Board.

Han, K.B., Kim, K.S., Lee, Y.J. and Park, S.K. (2003), "Analysis method for PSC-girder bridge deck slab with flexible girders", *J. Civil Eng.*, **7**(5), 515-524. https://doi.org/10.1007/BF02838317

Jeon, S.J., and Choi, M.S. and Kim, Y.J. (2012), "Graphical assessment for span ranges of psc girder bridges", *J. Bridge Eng.*, **17**(2), 343-352. https://doi.org/10.1061/(ASCE)BE.1943-5592.0000264

Kim, J.T., Park, J.H., Yoon, H.S. and Yi, J.H. (2007), "Vibration-based damage detection in beams using genetic algorithm", *Smart Struct. Syst.*, *Int. J.*, **3**(3), 263-280. https://doi.org/10.12989/sss.2007.3.3.263

Liu, C.Y. and DeWolf, J.T. (2007), "Effect of temperature on modal variability of a curved concrete bridge under ambient loads", *J. Struct. Eng.*, **133**(12), 1742-1751. https://doi.org/ 10.1061/(ASCE)0733-9445(2007)133:12(1742)

Mosavi, A.A., Seracino, R. and Rizkalla, S. (2012), "Effect of temperature on daily modal variability of a steel-concrete composite bridge", *J. Bridge Eng.*, **17**(6), 979-983. https://doi.org/10.1061/(ASCE)BE.1943-5592.0000372

Naito, H. and Bolander, J.E. (2019), "Damage detection method for RC members using local vibration testing", *Eng. Struct.*, **178**, 361-374. https://doi.org/10.1016/j.engstruct.2018.10.031

Oshima, Y., Yamamoto, K. and Sugiura, K.Y. (2014), "Damage assessment of a bridge based on mode shapes estimated by responses of passing vehicles", *Smart Struct. Syst.*, *Int. J.*, **5**(13), 731-753. https://doi.org/10.12989/sss.2014.13.5.731

Park, S., Stubbs, N., Bolton, R., Choi, S. and Sikorsky, C. (2001), "Field verification of the damage index method in a concrete box-girder bridge via visual inspection", *Comput.-Aided Civil Inf.*, **16**(1), 58-70. https://doi.org/10.1111/0885-9507.00213

Raja, B.N.K., Miramini, S., Duffield, C., Sofi, M., Mendis, P. and Zhang, L.H. (2020), "The influence of ambient environmental conditions in detecting bridge concrete deck delamination using infrared thermography (IRT)", *Struct. Control Health Monit.*, **27**, e25064. https://doi.org/10.1002/stc.2506

Rehman, S.K., Ibrahim, Z., Memon, S.A. and Jameel, M. (2016), "Nondestructive test methods for concrete bridges: A review", *Constr. Build Mater.*, **107**(2016), 58-86. https://doi.org/10.1016/j.conbuildmat.2015.12.011

Shokrani, Y., Dertimanis, V.K., Chatzi, E.N. and Savoia, M.N. (2018), "On the use of mode shape curvatures for damage localization under varying environmental conditions", *Struct. Control Health Monit.*, **25**, e2132. https://doi.org/10.1002/stc.2132

Timoshenko, S. and Woinowsky-Krieger, S. (1959), *Theory of Plates and Shells*, McGraw-Hill, New York, USA.

Tributsch, A. and Adam, C. (2018), "An enhanced energy vibration-based approach for damage detection and localization", *Struct. Control Health Monit.*, **25**, e2047. https://doi.org/10.1002/stc.2047

Wahab, M.A. and Roeck, G. (1997), "Effect of temperature on dynamic system parameters of a highway bridge", *Proc. Struct. Eng. Int.*, **7**(4), 266-270. https://doi.org/ 10.2749/101686697780494563

Xiang, Z.H., Dai, X.W., Zhang, Y. and Lu, Q.H. (2010), "The tap-scan method for damage detection of bridge structures", *Interact. Multiscale Mech.*, **3**(2010). https://doi.org/10.12989/imm.2010.3.2.173

Yan, Y.J., Cheng, L., Wu, Z.Y. and Yam, L.H. (2007), "Development in vibration-based structural damage detection technique", *Mech. Syst. Signal Pr.*, **21**(5), 2198-2211. https://doi.org/10.1016/j.ymssp.2006.10.002

Yang, Y.B. and Yang, J.P. (2004), "State-of-the-art review on modal identification and damage detection of bridges by moving test vehicles", *Int J Struct Stab Dyn*, **18**(2), 1850025. https://doi.org/10.1142/S0219455418500256

Yang, Y.B., Lin, C.W. and Yau, J.D. (2004), "Extracting bridge frequencies from the dynamic response of a passing vehicle", *J. Sound Vib.*, **272**(3-5), 471-493. https://doi.org/10.1016/S0022-460X(03)00378-X

Yang, Y.B., Li, Y.C. and Chang, K.C. (2014), "Constructing the mode shapes of a bridge from a passing vehicle: a theoretical study", *Smart Struct. Syst.*, *Int. J.*, **13**(5), 797-819. https://doi.org/10.12989/sss.2014.13.5.797

Yang, D.H., Yi, T.H. and Li, H.N. (2017), "Coupled fatigue-corrosion failure analysis and performance assessment of RC bridge deck slabs", *J. Bridge Eng.*, **22**(10), 04017077. https://doi.org/10.1061/(ASCE)BE.1943-5592.0001108

Zhang, Y., Wang, L.Q. and Xiang, Z.H. (2012), "Damage detection by mode shape squares extracted from a passing vehicle", *J. Sound Vib.*, **331**(2), 291-307. https://doi.org/10.1016/j.jsv.2011.09.004

Zhu, J.Y. and Popovics, J.S. (2007), "Imaging concrete structures using air-coupled impact-echo", *J. Eng. Mech.*, **133**(6), 628-640. https://doi.org/10.1061/(ASCE)0733-9399(2007)133:6(628)

BS